(Manuscript ID: 3DP-2023-0150.R2)

Submission to ***3D Printing and Additive Manufacturing***

3D Bioprinting of Graphene Oxide-incorporated Hydrogels for Neural Tissue Regeneration

Jiahui Lai [1], Xiaodie Chen [1], Helen H. Lu [2], Min Wang [1, *]

[1] Department of Mechanical Engineering
The University of Hong Kong
Pokfulam Road, Hong Kong

[2] Department of Biomedical Engineering
Columbia University
1210 Amsterdam Avenue, New York, NY10027, U.S.A.

Keywords: *3D bioprinting, hydrogel scaffold, graphene oxide, neural tissue engineering, mesenchymal stem cell*

* Corresponding Author:
Professor Min Wang, at The University of Hong Kong, Hong Kong
Email: memwang@hku.hk Tel: +852 3917 7903 Fax: +852 2858 5415

Abstract

Bioprinting has emerged as a powerful manufacturing platform for tissue engineering, enabling the fabrication of 3D living structures by assembling living cells, biological molecules and biomaterials into these structures. Among various biomaterials, hydrogels have been increasingly used in developing bioinks suitable for 3D bioprinting for diverse human body tissues and organs. In particular, hydrogel blends combining gelatin and gelatin methacryloyl (GelMA) ("GG hydrogels") receive significant attention for 3D bioprinting owing to their many advantages such as excellent biocompatibility, biodegradability, intrinsic bioactive groups, and polymer networks that combine the thermo-responsive gelation feature of gelatin and chemically crosslinkable attribute of GelMA. However, GG hydrogels have poor electroactive properties, which hinders their applications in neural tissue engineering where electrical conductivity is required. To overcome this problem, in this study, a small amount of highly electroactive graphene oxide (GO) was added in GG hydrogels to generate electroactive hydrogels for 3D bioprinting in neural tissue engineering. The incorporation of GO nanoparticles slightly improved mechanical properties and significantly increased electrical conductivity of GG hydrogels. All GO/GG composite hydrogels exhibited shear thinning behavior and sufficient viscosity and hence could be 3D printed into 3D porous scaffolds with good shape fidelity. Furthermore, bioinks combining rat bone marrow-derived mesenchymal stem cells (rBMSCs) with GO/GG composite hydrogels could be 3D bioprinted into GO/GG constructs with high cell viability. GO nanoparticles in the constructs provided UV shading effect and facilitated cell survival during UV exposure after bioprinting. The GO/GG composite hydrogels appear promising for 3D bioprinting applications in repairing damaged neural tissues.

1. Introduction

The concept of 3D bioprinting was officially unveiled at the first bioprinting international conference in 2004,[1] in which biomaterials, biological molecules and living cells are laid down together in a layer-by-layer manner to construct unique 3D living structures.[2-4] Over the past two decades, 3D bioprinting has made rapid progresses and has now become a powerful biofabrication platform for different biomedical applications such as drug screening,[5,6] tissue and organ models,[7-9] and tissue engineering.[10-14]

Hydrogels of natural biopolymers are attractive biomaterials which are now commonly used for 3D bioprinting due to their many and distinctive advantages. One such hydrogel is gelatin, which is derived from collagen and possesses excellent biocompatibility with intrinsic Arg-Gly-Asp (RGD) motifs and accessible active groups for promoting cell attachment and growth. Gelatin exhibits a temperature-sensitive reversible gelation process: it is in the gel-state at a low temperature (< 29 ºC) and becomes a low-viscosity liquid at a temperature higher 37 ºC. Therefore, gelatin cannot maintain its structural integrity and will quickly lose its mass when used *in vivo*, which severely limits its use in bioprinting applications. There are several strategies to deal with the issue of unstable structures of gelatin. A common strategy is chemical modification of gelatin with the methacryloyl (MA) group, thereby endowing gelatin with the photo-crosslinking ability. After chemical crosslinking, gelatin methacryloyl (GelMA) can maintain the shape of printed structures in the human physiological environment.[15-17]

The central nervous system (CNS) in human bodies is vitally important as it regulates physiological functions and controls body activities.[18] This regulation relies on electrical signal transmission from the brain through CNS and peripheral nervous system (PNS) to various parts of the body via a complex network of nerves and neural cells. The native neural

tissue exhibits a complex layered architecture with very soft mechanical properties having an average modulus at the kPa level.[19,20] Therefore, materials used for neural tissue engineering should be very soft and ideally have certain degree of electrical conductivity. The mechanical properties of GelMA hydrogels can be controlled by adjusting its concentration and crosslinking degree. A low concentration of GelMA can provide a relatively soft mechanical stiffness that is more suitable for repairing neural tissues. But it will face the problem of low viscosity, which makes it very difficult to be printed into 3D structures with good shape fidelity. The combination of gelatin and GelMA can form Gelain/GelMA (GG) hydrogel blends with good printability and soft mechanical properties. For a GG hydrogel blend, gelatin provides high viscosity during the bioprinting process and can be removed from the hydrogel blend during *in vitro* incubation at 37 ºC, while GelMA can maintain the printed structures after photocrosslinking. It has been reported that GG hydrogels could be bioprinted into cell-laden scaffolds with controlled architectures and geometry.[21,22] However, GG hydrogels lack the electrical conductivity required for successfully regenerating neural tissues. One way to integrate electroactive properties into hydrogels is to add a small amount of highly conductive nanomaterial, such as graphene oxide or carbon nanotubes, in the hydrogels.[23-25]

Graphene oxide (GO) is a popular carbon nanomaterial that possesses many distinctive physiochemical properties, including biocompatibility, carbon domains, hydrophilic functional groups, excellent electron mobility, and high surface-to-volume ratio.[26-28] It was reported that GO could induce the differentiation of stem cells towards many somatic cell lineages, such as chondrogenic type,[27] myogenic type[29] and osteogenic type.[30-32] GO may be highly dispersed in aqueous solutions, making it suitable for integration into hydrogels.[23,32-34] The addition of GO into GG hydrogels should yield composite hydrogels with good

electroactivity, printability, crosslinking ability, and appropriate softness for 3D bioprinting for neural tissue engineering.

In this work, GG-based hydrogels were developed for 3D bioprinting in neural tissue engineering by combining GO, gelatin, and GelMA. GO/GG composite hydrogels with different GO contents were made and then characterized in terms of their light transmission, mechanical properties, swelling ratio and electrical conductivity. The printability of GO/GG hydrogels with different GO concentrations were evaluated by studying rheological properties of hydrogels and shape fidelity of 3D printed structures. Rheological properties concerned shear viscosity and gravity-induced flow behavior, while shape fidelity was evaluated using 3D printed single-layer and multilayer structures. Finally, rat bone marrow-derived mesenchymal stem cells (rBMSCs) were added into GO/GG composite hydrogels to formulate bioinks, which were subsequently processed into 3D cell-laden constructs using a micro extrusion-based 3D bioprinting system. The cell-laden GO/GG constructs were incubated *in vitro* and the effects of GO on cell behaviour were studied.

2. Materials and Methods

2.1. Materials and synthesis of GelMA

Graphene oxide (GO, consisting of 15-20 sheets and being 4-10% edge-oxidized) and gelatin (type A, from porcine skin) were purchased from Sigma-Aldrich, USA. All other materials were also Sigma-Aldrich products and were used without further purification. GelMA was synthesized according to the established protocol.[35] Briefly, methacrylic anhydride (MA, 0.6 g of MA per 1 g of gelatin) was added to a gelatin solution (10% (w/v)) at 50 ºC for reaction for 1 h, followed by dialysis and freeze-drying to obtain dried GelMA samples.

2.2. Fabrication and characterization of GO/GG composite hydrogels

2.2.1 Fabrication of GG composite hydrogels

A GG hydrogel blend containing 5% (w/v) gelatin and 5% (w/v) GelMA was firstly prepared by dissolving specific quantities of gelatin and GelMA in DI water at 50ºC. Afterwards, a certain amount of GO and 0.25% (v/v) photoinitiator (2-Hydroxy-2-methylpropiophenone) were added into the GG hydrogel and mixed magnetically to achieve a homogeneously distribution of GO in the GO/GG composite hydrogel.

2.2.2 Light transmission

The light transmission of GO/GG composite hydrogels with GO concentrations ranging from 0~0.1 % (w/v) was analysed based on light transmittance spectra, which were obtained using a Shimadzu spectrophotometer (UV2600, Shimadzu, Japan) in the wavelength range of 330–1,000 nm.

2.2.3 Compressive properties

Samples for compressive tests of GO/GG composite hydrogels were prepared by casting them into disks with an average diameter of 10 mm and a height of 4 mm. The actual initial dimensions (diameter and thickness) of each sample were measured using a digital caliper. The compressive tests were performed using a mechanical testing machine (Instron 5848, UK) at room temperature (n=5 for each type of GO/GG hydrogels). The compressive modulus of samples was calculated from the recorded stress-strain curves using the software Bluehill.

2.2.4 Swelling ratio

The swelling ratio of GO/GG hydrogels with different GO concentrations was calculated by the ratio of the swollen weight and dried weight. Briefly, hydrogel samples (n=3 for each type of samples), which were cast disks with a diameter of about 10 mm and a height of

about 4 mm, were firstly dried, and the dried weight (W_d) was recorded. The dried samples were then put into PBS for 24 hours to allow them to reach the equilibrium swelling state, and the swollen weight (W_s) was recorded. Finally, the swelling ratio of each sample was calculated as W_s/W_d.

2.2.5 Electrical conductivity

The electrical conductivity (σ) of hydrogel samples (n=3 for each type of GO/GG hydrogels) was calculated using the following equation:

$$\sigma = \frac{L}{RA} \tag{1}$$

where L, R, and A were the length, electrical resistance, and cross-sectional area, respectively, of the sample. Briefly, GO/GG hydrogels with different GO contents were cast into disks with an average diameter of 10 mm and a height of 3 mm. The electrical resistance (R) of each sample was measured using a multimeter system (DAQ6510 Data Acquisition/Multimeter System, Keithley, USA). The electrical conductivity of each sample was then calculated using Eq. (1).

2.3. Printability of GO/GG composite hydrogels

2.3.1 Rheological properties

Two types of rheological tests were conducted for GO/GG hydrogels: (1) shear viscosity, and (2) gravity-induced flow. The shear viscosity was measured at 20 ºC (i.e., the 3D printing temperature) in a shear rate range of 0.01-1000 1/s using a rotational rheometer (MCR302, Anton Paar, Austria) with a 25 mm parallel plate and 0.55 mm measurement gap. The gravity-induced flow behaviour was studied by inverting individual tubes containing different GO/GG hydrogels for 10 minutes.

2.3.2 Shape fidelity of 3D printed grids

To examine the shape fidelity of 3D printed structures, each type of GO/GG composite hydrogels was printed as single-layer grids and eight-layer grids using an extrusion-based 3D bioprinter (3D Discovery™, regenHU Ltd, Swizerland). The 3D printed single-layer grids were observed using an optical microscope (Leica DMi8, Germany), while the 3D printed eight-layer grids were captured using a digital single lens mirrorless camera (Z6, Nikon, Japan).

2.3.3 Structural morphology of 3D printed structures

The structural morphology of 3D printed GO/GG structures was observed using a field emission scanning electron microscope (Hitachi S3400N VP SEM, Japan). Briefly, 3D printed structures were frozen at -80 ºC overnight, followed by freeze-drying for 3 days. The freeze-dried samples were sputter-coated with a thin layer of gold before SEM observation. SEM images were taken for each sample, capturing the top and side views of the sample.

2.4. 3D bioprinting of cell-laden constructs

2.4.1 Cell and cell culture

rBMSCs were used in the current study. They were firstly cultured in a culture medium consisting of Dulbecco's modified Eagle's medium (DMEM, Gibco, USA), 10% fetal bovine serum (FBS, Gibco, USA), and 100 U/ml penicillin-streptomycin (Gibco, USA). *In vitro* cell culture was performed in a humidified incubator at 37 °C with 5% CO_2. When cells reached 80%–90% confluence, they were detached, counted, and subjected to making GO/GG bioinks for the subsequent 3D bioprinting.

2.4.2 3D bioprinting

Fig. 1 illustrates the whole 3D bioprinting process using rBMSC/GO/GG bioinks. The first step was to design tissue engineering scaffolds in the computer-aided design (CAD) environment according to the application requirements. In this work, a grid structure was designed using the BioCAD software of the 3D bioprinter (RegenHU, Swizerland). After designing the bioprinting path, the next step was to prepare bioinks. Briefly, 0.2 g of gelatin and 0.2 g of GelMA were dissolved in 2 ml of DI water at 50 ºC to obtain GG hydrogel blends. A certain amount of GO and photoinitiator were then added into GG hydrogel blends to make GO/GG composite hydrogels. The uncrosslinked and acellular GO/GG hydrogels were sterilized at room temperature by ^{60}Co γ-irradiation for 20 min. Afterwards, the sterilized 2 ml GO/GG hydrogel was heated to 37 ºC for it to change to the liquid state and then mixed with 2 ml of a cell suspension (at 2 ×10^6 cell/ml). The hydrogel-cell suspension mixture was mildly stirred for achieving a homogenous cell distribution in the mixture, i.e., the bioink. The prepared rBMSC/GO/GG bioinks with different GO concentrations were loaded into syringes for subsequent bioprinting uses. When the printing path and bioinks were ready, 3D bioprinting was performed using a piston-based extrusion 3D bioprinter (3D Discovery™, regenHU Ltd, Swizerland). Regarding bioprinting parameters, the printing speed was set at 8 mm/s, the printing temperature was 20 ºC, the piston speed was 0.02 to 0.03 mm/s, and the inner diameter of the printing head was 0.26 mm. Immediately after bioprinting, cell-laden constructs were crosslinked using a 365 nm UV irradiation with a power of 360 mW for 3 minutes. Finally, all bioprinted constructs were immersed in the cell culture medium and cultured in an incubator for *in vitro* development.

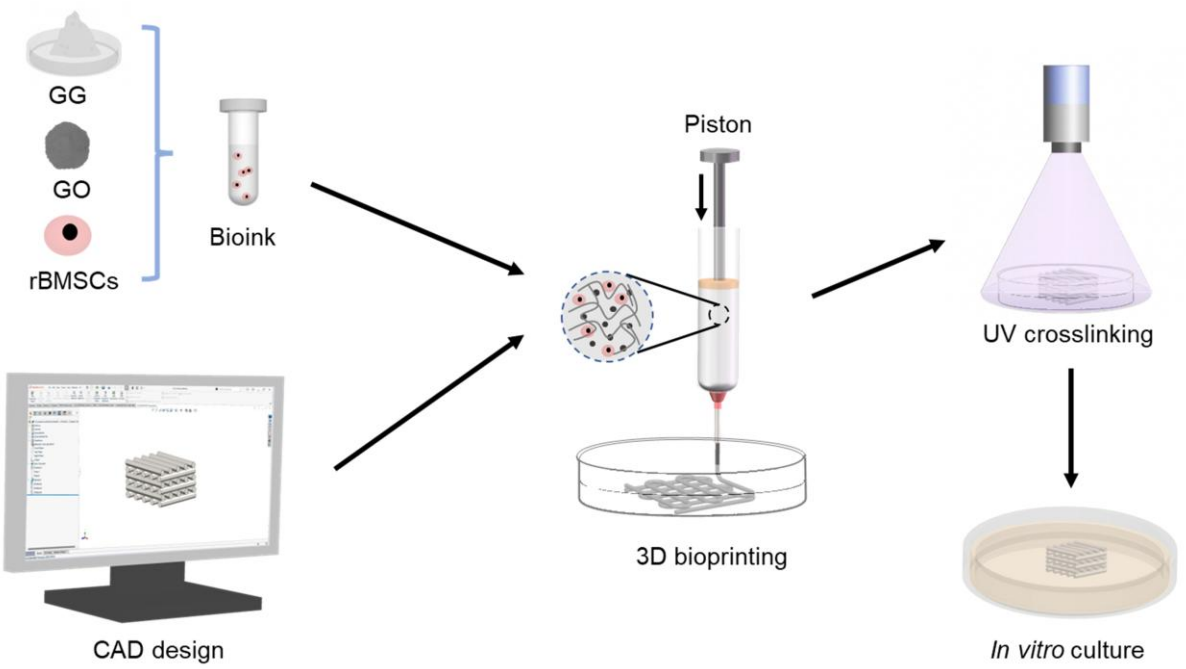

Figure 1 Schematic diagram showing 3D bioprinting of cell-laden constructs with controlled architectures using bioinks composed of GG, GO and rBMSCs.

2.4.3 Cell behaviour

The viability of rBMSCs incorporated in bioprinted GO/GG structures was examined using Live/Dead assay. In live/dead cell staining, live cells were stained with calcein AM and would show green fluorescence under the microscope, whereas dead cells were stained with ethidium homodimer EthD-1 and would show red fluorescence. At specific culture time points, bioprinted cell-laden constructs were taken out and washed three times using sterilized PBS, followed by adding Live/Dead staining solution and then incubation at room temperature for 30 minutes. Afterwards, the stained cell-laden constructs were observed under a fluorescence microscope (Leica DMi8, Germany) and at the same time, fluorescence images were taken for each cell-laden sample.

2.5. Statistical analysis

All numerical data was presented as mean ± standard deviation (S.D.). Statistical analysis was performed via one-way ANOVA using a post-hoc analysis of least significant difference (LSD), with a single asterisk (*) representing a significant difference ($p < 0.05$) between experimental groups.

3. Results and Discussion

3.1. Characteristics of GG-based hydrogels

GG-based hydrogels with different GO concentrations were characterized in terms of their light transmission, compressive properties, swelling ratio, and electrical conductivity. Fig. 2a displays the light absorbance curves of different GG-based hydrogels under UV light in the wavelength range of 330-1000 nm. The addition of GO was found to reduce the transparency of GG hydrogels and increase light absorbance. It could be seen that the more the GO addition, the more the light absorbance. Fig. 2b shows compressive modulus of GO/GG composite hydrogels. It was reported in previous work by others that GG hydrogels possessed a mechanical strength in the magnitude of 10 kPa or higher.[36,37] Although the addition of GO improved the mechanical properties, the current study showed that the compressive modulus of GG-based hydrogels remained in the kPa range, indicating these composite hydrogels were relatively soft materials. Fig. 2c presents swelling ratio of GG-based hydrogels, showing that the inclusion of GO slightly decreased the swelling ratio of GG hydrogels and that the higher the GO content, the smaller the swelling ratio. This may be attributed to that GO nanoparticles had entered the polymer networks and occupied the space in GG hydrogels, resulting in the decreased swelling ratio. Fig. 2d demonstrates that the electrical conductivity increased with an increase in GO amount for GO/GG hydrogels. It was also revealed that even a small amount of GO nanoparticles could significantly improve the electrical

conductivity of GG-based hydrogels, which is attributed to the superior electron mobility of GO.[23,38]

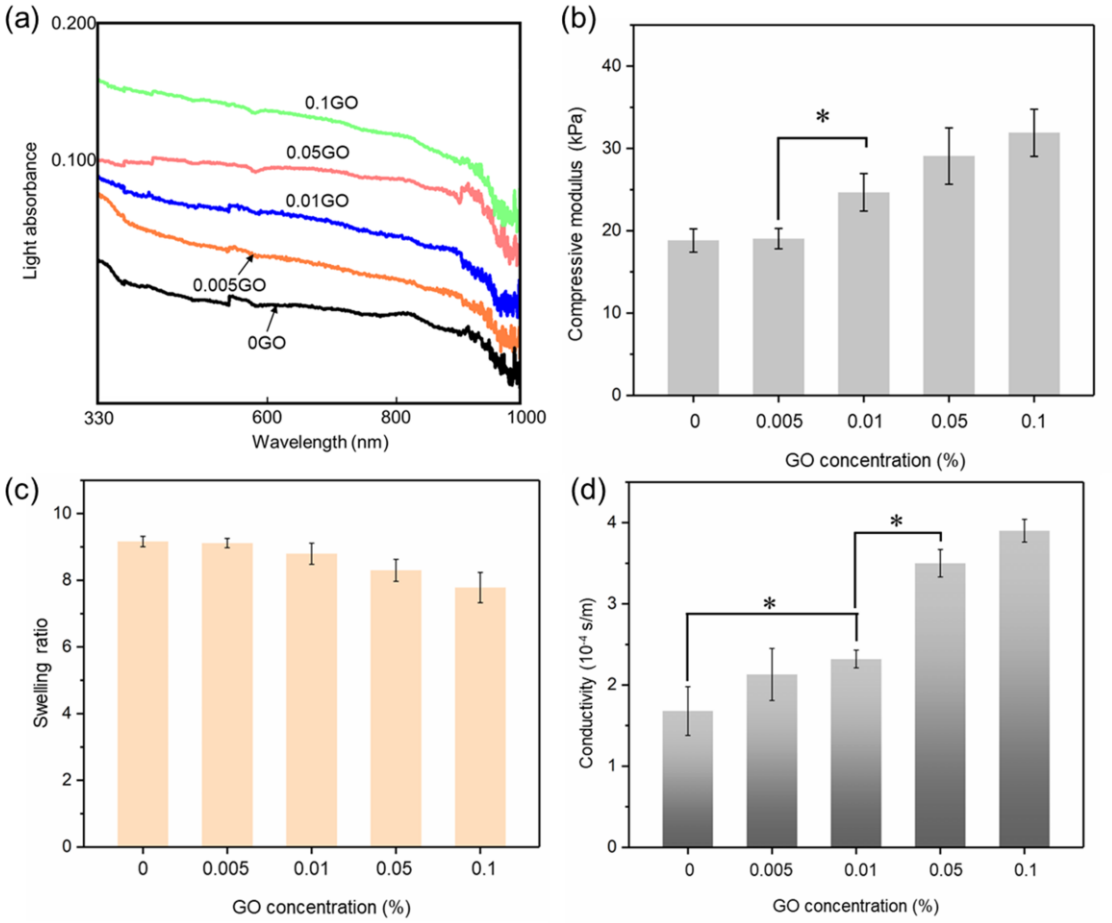

Figure 2 Characteristics of GO/GG composite hydrogels with different GO contents: (a) light absorption; (b) compressive modulus; (c) swelling ratio; (d) electrical conductivity.

3.2. Printability of GG-based hydrogels

The printability of GG-based hydrogels was investigated in terms of shear viscosity and gravity-induced flow of these hydrogels, and shape fidelity and structural morphology of 3D printed structures. The shear viscosity of GG-based hydrogels with different GO contents is shown as Fig. 3a. All tested hydrogels exhibited a decrease in viscosity with an increase in shear rate, indicating a shear-thinning behavior which is crucially required for the successful

extrusion of a hydrogel by a 3D printer. This property enabled GO/GG hydrogels to maintain high viscosity and stability before shear stress was applied and to greatly reduce the viscosity for the ink to behave as a liquid under a high stress when going through the printing head, leading to smooth extrusion of the hydrogel. Additionally, the inclusion of GO slightly increased the viscosity of GG-based hydrogels, which was beneficial for extrusion-based 3D bioprinting. Fig. 3b reveals gravity-induced hydrogel flow behavior when the test tubes containing different GO/GG hydrogels were inverted. It can be seen that all hydrogels could stay stable in inverted test tubes without downward flow, indicating that these hydrogels had sufficient viscosity to remain static before a high shear rate was applied. Also, it was apparent that the color of GO/GG composite hydrogels became increasingly darker when the GO content increased (from (i) to (v) in Fig. 3b).

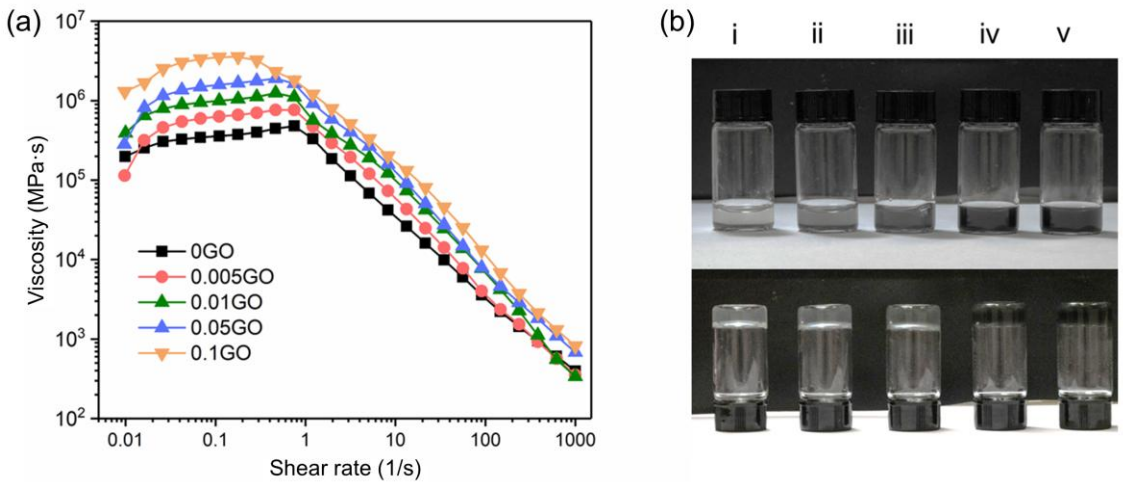

Figure 3 Rheological properties of GO/GG composite hydrogels: (a) shear viscosity, and (b) gravity-induced flow behaviour of composite hydrogels with (i) 0%, (ii) 0.005%, (iii) 0.01%, (iv) 0.05%, and (v) 0.1% of GO (Bottom row: inverted test tubes containing composite hydrogels.).

The shape fidelity of 3D printed single-layer and multilayer hydrogel grids was examined at different levels: macroscopic and microscopic. Fig. 4a provides optical microscope (OM)

images of 3D printed single-layer grids (18×18 mm^2 in size) using different GO/GG composite hydrogels. From low magnification (×4) OM images, it can be seen that these hydrogels could be printed into 2D grids with regular macropores. From zoomed view of these OM images, black GO nanoparticles were seen to be homogeneously distributed within the GG hydrogel matrix. Fig. 4b are photos of 3D printed eight-layer grids (18×10×3.2 mm^3 in size) from different GO/GG composite hydrogels, showing the top, oblique and side views of these grids. It could be said that GO/GG hydrogels after 3D printing could maintain good shape fidelity with delicate internal structures, indicating good printability and stackbility of GO/GG hydrogels. These 3D printed eight-layer GO/GG hydrogel grids were also studied under SEM. With the top view (Fig. 5a), 3D printed grids exhibited precise and regular macro-pores, while looking from the side (Fig. 5b), 3D printed grids exhibited less porous structures. Overall, these GO/GG hydrogels had adequate viscosity for 3D printing into 3D porous objects with good internal structures, suggesting good printability of GO/GG hydrogels for extrusion-based 3D bioprinting.

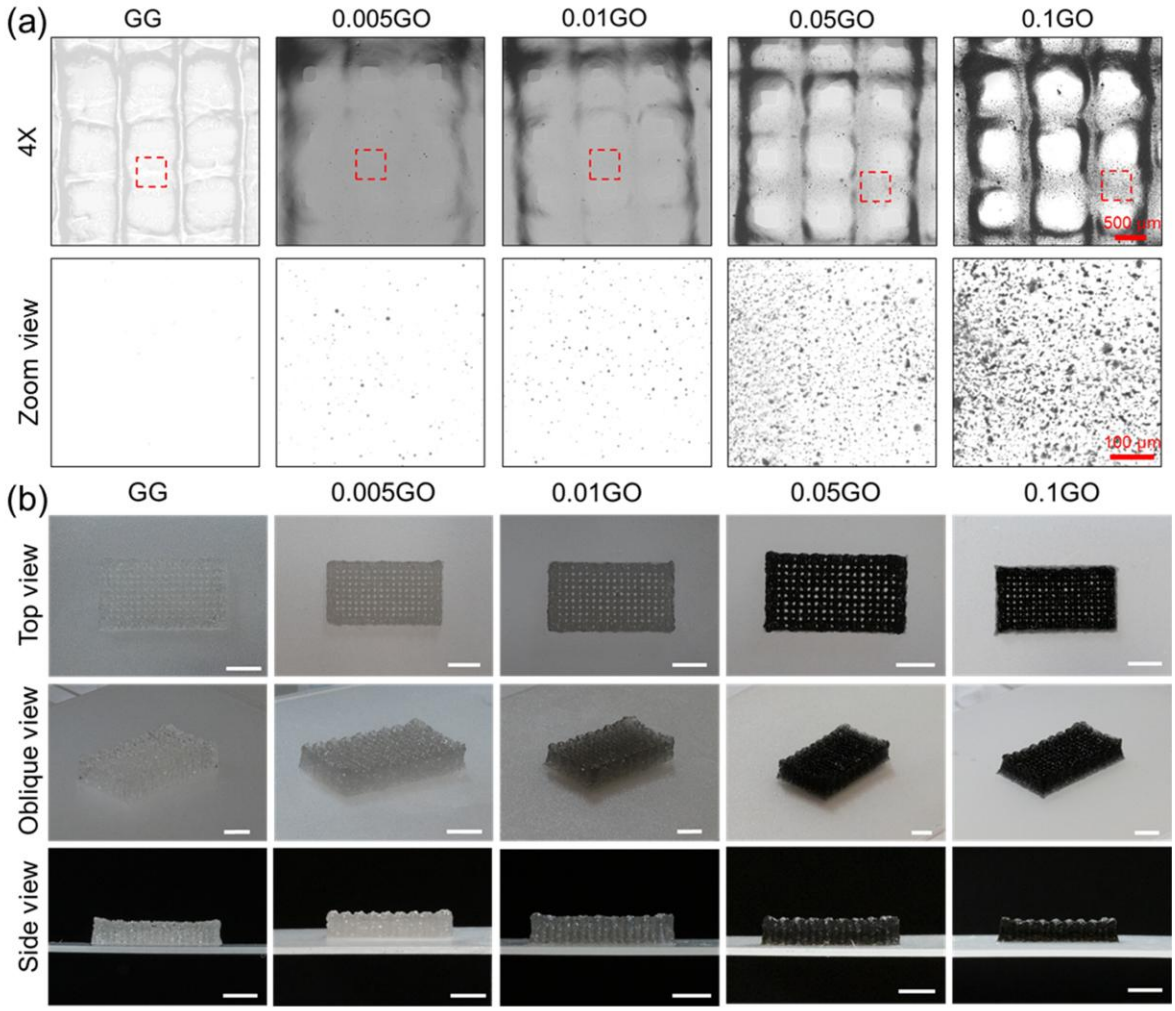

Figure 4 Shape fidelity of 3D printed porous structures using GO/GG composite hydrogels with different GO contents: (a) optical microscope images of 3D printed single-layer grids, (b) photographs of 3D printed eight-layer grids (scale bar: 5 mm).

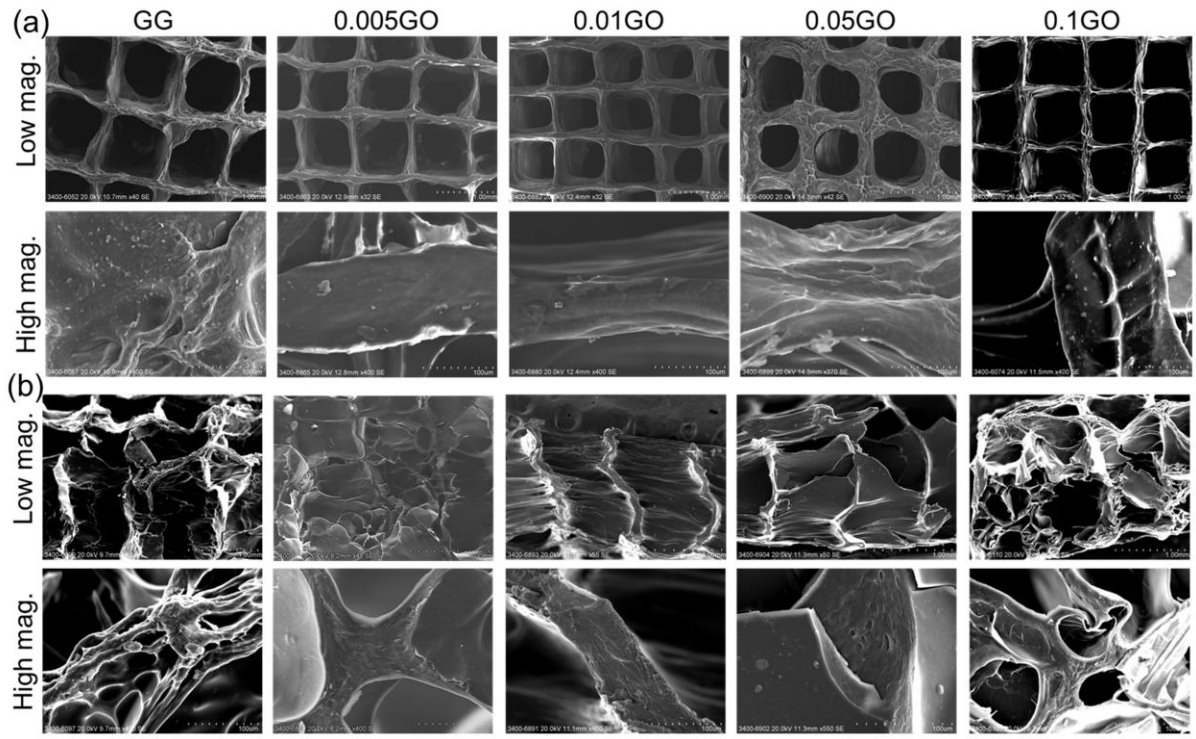

Figure 5 SEM images of 3D printed porous GO/GG structures using GO/GG composite hydrogels with different GO contents: (a) top view, and (b) side view, at a low magnification (top row) and at a high magnification (bottom row).

3.3 Cells in 3D bioprinted cell-laden constructs

rBMSC-containing GG hydrogels without GO or with 0.01% (w/v) or 0.1% (w/v) GO were processed into cell-laden constructs via micro extrusion-based 3D bioprinting. These cell-laden hydrogel constructs were 3D grids (20×15×0.4 mm^3 in size), which were subjected to UV crosslinking for stabilizing the printed structures. The viability of rBMSCs in 3D bioprinted cell-laden constructs was evaluated at day 1 and day 7 of culture using Live/Dead assay, and the results are shown in Fig. 6. In the Live/Dead fluorescence images, living cells were in green colour and dead cells were in red colour. The Live/Dead cells was counted using the ImageJ software for subsequent calculations to quantify cell viability (n=3 for each type of cell-laden structures). At day 1, the composite hydrogel with 0.1 % (w/v) of GO showed the highest cell viability (> 90%), followed by the composite hydrogel with 0.01 %

(w/v) of GO, with both hydrogels rendering higher cell viability than pure GG hydrogel. Interestingly, at day 7, the cell viability for all GG-based hydrogel scaffolds increased to a similar level, while the cell viability for pure GG hydrogel showed the largest increase from about 60% to about 90%, suggesting that GO/GG composite hydrogels provided good support for cell survival and growth. For micro-extrusion-based 3D bioprinting, cell viability in GG-based hydrogels could be significantly influenced by the high shear stress imposed on hydrogels when they passed through the narrow passage in the printing head and also by the detrimental impact of UV irradiation during chemical crosslinking of GelMA.[39-41] As a result, at day 1, the viability of rBMSCs within GO/GG hydrogels was relatively low compared to that at day 7. Moreover, it could be seen that the inclusion of GO in GG hydrogels improved cell survival during the 3D bioprinting process and maintained significantly higher cell viability than GG hydrogel without GO addition. These findings demonstrated the benefits of GO inclusion in hydrogels for promoting cell survival and growth during and after 3D bioprinting.

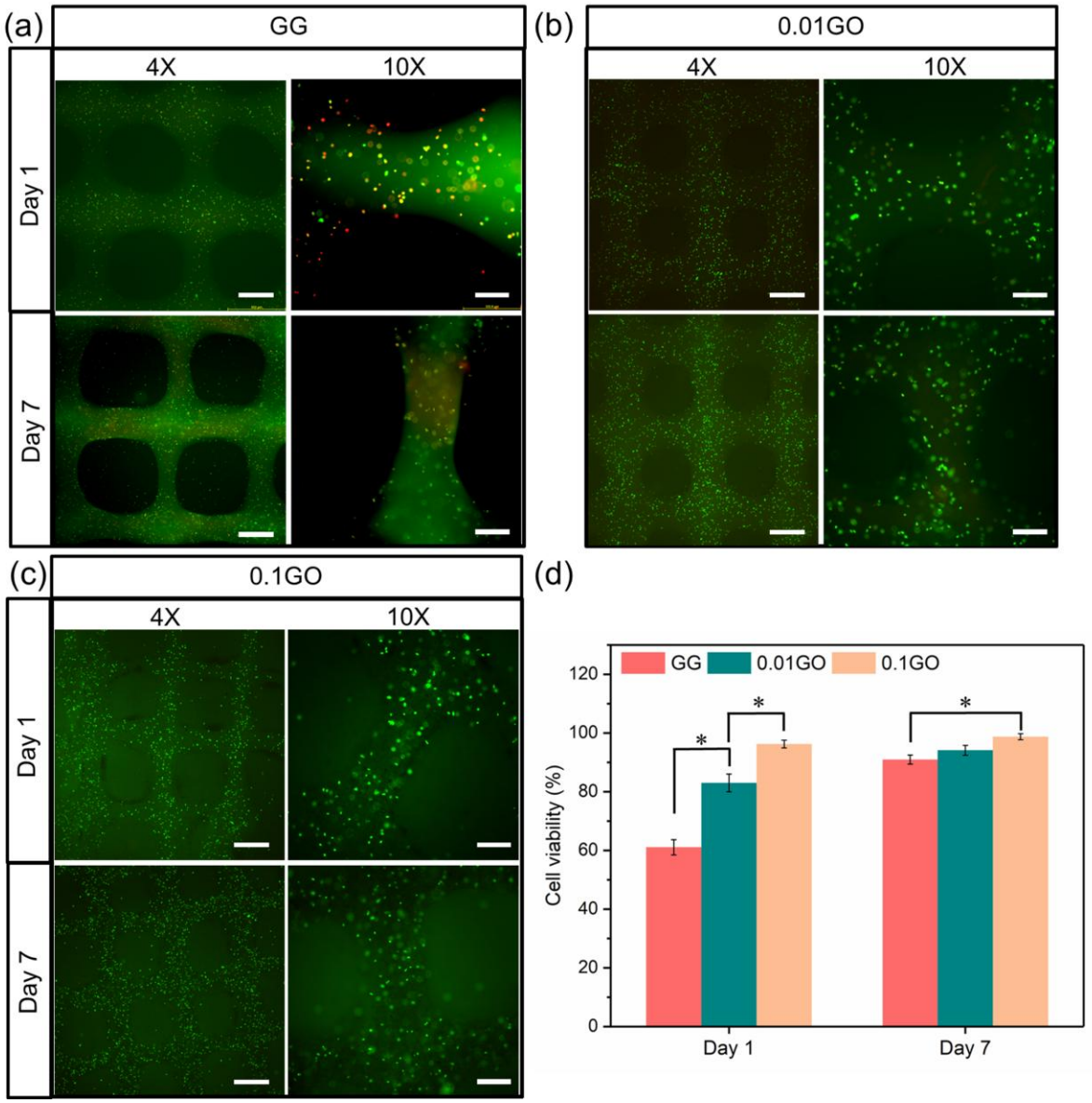

Figure 6 Live/Dead fluorescence images of 3D bioprinted cell-laden constructs made from (a) GG hydrogel, (b) GO/GG composite hydrogel with 0.01% (w/v) of GO, (c) GO/GG composite hydrogel with 0.1% (w/v) of GO (scale bar: 500 μm for 4× and 200 μm for 10×), and (d) quantitative cell viability.

GG hydrogels are highly appealing biomaterials for 3D bioprinting owing to their distinctive advantages such as excellent biocompatibility, biodegradability, and intrinsic RGD motifs. Furthermore, GG hydrogels can possess good extrudability, printability, and structural stability, which are required for successful micro extrusion-based 3D bioprinting, because of

the complementary polymer networks of gelatin and GelMA. The thermo-responsive gelatin network provides good viscosity and extrudability for 3D bioprinting, while the photocrosslinkable GelMA network allows bioprinted constructs to be stabilized via chemical crosslinking. However, GG hydrogels are non-conductive, which hinders their application in neural tissue engineering where electroactivity is required or preferred. To overcome this problem, in the current study, highly electroactive GO was added to GG hydrogels to provide and improve their electrical conductivity. The effects of GO on properties of GG hydrogels were systematically investigated regarding their rheological properties, printability, electrical conductivity, swelling ratio, mechanical properties, and biological properties. The experimental results have shown that the incorporation of GO significantly enhanced the electrical conductivity of GG hydrogels, while slightly decreasing the swelling ratio as the GO nanoparticles had occupied some space existing in the GG hydrogel networks. The addition of GO also improved the compressive modulus of GG hydrogels but the modulus still remained at the kPa level. Furthermore, the presence of black GO nanoparticles caused GG hydrogels to get darken, resulting in reduced light transmission. While it is important to have adequate amount of GO in GG hydrogels to obtain sufficient conductivity for applying GO/GG composite hydrogels in neural tissue engineering, an increase in GO amount in hydrogels reduces UV light transmission, causing difficulties in crosslinking GelMA in GG hydrogels. Therefore, a balance has to be made with regard to the GO amount in GG hydrogels. In the current study, it appeared that 0.1% of GO could be added in GG hydrogels, which helped to increase electrical conductivity of composite hydrogels while not adversely affecting the crosslinking efficiency and degree of GelMA. This amount of GO for the composite hydrogel had produced the attributes of hydrogels that are required for 3D bioprinting of GG-based hydrogels in neural tissue engineering.

GO/GG composite hydrogels displayed favourable rheological properties for 3D bioprinting, including shear thinning behaviour and adequate viscosity, making them suitable for the 3D bioprinting technology used in the current study. With our state-of-the-art 3D bioprinter, GO/GG hydrogels were printed into single-layer and multilayer 3D grids with good shape fidelity. These 3D printed GO/GG grids showed delicate porous structures without collapsing during and after printing, demonstrating good printability of GO/GG hydrogels that the current study aimed to achieve.

rBMSCs were incorporated in GO/GG composite hydrogels to produce rBMSCs/GO/GG bioinks, which could be bioprinted successfully into cell-laden scaffolds with high cell viability. The viability of living cells within a bioprinted construct is a critical issue for micro extrusion-based 3D bioprinting or any other bioprinting technology. In extrusion-based bioprinting, cell viability is affected by several bioprinting parameters, such as pneumatic pressure, nozzle size (i.e., nozzle inner diameter), shear stress and UV crosslinking dosage.[36,39,42,43] Furthermore, a few other factors such as hydrogel type (alginate, hyaluronic acid, gelatin, etc.) can also influence cell viability. For example, the viability of cells within Matrigel (which consists of four major basement membrane ECM proteins: laminin (~60%), collagen IV (~30%), entactin (~8%) and the heparin sulfate proteoglycan perlecan (~2–3%)), alginate (2%), agarose (1%), and Pluronic® F-127 (25%) was compared over culture time during *in vitro* culture experimemts.[44] After five-hour *in vitro* incubation, there was no significant difference for cells among these hydrogels. However, after seven days of culture, cells in Matrigel and alginate stayed at about 90% cell viability, while the cell viability for agarose decreased to about 70% and no cell survived in Pluronic® F-127. GG hydrogel were shown in previous reports by others to be appropriate for supporting cell growth *in vitro* and *in vivo* in the long term.[15,22,36,37] However, in this study, it was observed that cell viability for the GG hydrogel was considerably reduced after 3 minutes of UV exposure, going down to

the 60% level of cell viability at day 1 of culture; whereas cell viability for GO/GG hydrogels was much higher than that of GG hydrogels. High shear stress could decrease cell viability for extrusion-based 3D bioprinting. However, as the added small amount of GO slightly increased the viscosity of GG hydrogels, they should not lower down shear stress exerted on the cells and hence would not cause such a big difference in cell viability. Considering this, such significantly reduced cell viability for GG hydrogels possibly had primarily resulted from the detrimental effect of UV irradiation.[40,43] Colosi *et al*. reported that an increased UV exposure time decreased cell viability.[45] In another study, Billiet *et al.* increased irradiation dose of UV (365 nm) from 1350 mJ cm^{-2} to 5400 mJ cm^{-2} for extruded GelMA constructs, which significantly reduced the viability of Hep-G2 cells from 90% to 56%.[46] If the UV exposure dose had exceeded a threshold, UV light would have caused significant cell death in the current bioprinting process. This problem may be dealt with by reducing the UV exposure time.[47] However, a reduction in UV irradiation dose could result in incomplete crosslinking of GelMA, leading to instability and rapid biodegradation of bioprinted GelMA structure, as was evident in our previous study.[36] Possible ways to minimize UV-induced damage of cells include changing the type and concentration of photoinitiator or utilizing a more benign wavelength of light instead of UV light. Interestingly, in this study, it was found that even a small amount of GO could greatly improve the ability of living cells in GO/GG hydrogels to survive the UV exposure. After 1-day incubation, the cell viability was above 90% for 0.1GO/GG hydrogel, about 80% for 0.01GO/GG hydrogel, and at 60% for GG hydrogel. The greatly improved cell viability in GO/GG hydrogels is mainly attributed to that the UV shading effect (i.e., UV absorption) of GO had reduced the direct exposure of UV on living cells in the hydrogels, leading to less damage to cells by UV irradiation, which was also demonstrated in a previous study for GO/GelMA hydrogels containing fibroblasts.[41] Neural cells, such as astrocytes and PC12 cells, have shown good viability and growth in GelMA-

based hydrogels.[23,37] With the benefits of added GO, GO/GG hydrogels are expected to facilitate the survival, growth and functionality of neural cells during bioprinting and also post-bioprinting incubation. Overall, the GO/GG composite hydrogels possessed enhanced printability, mechanical properties, and electrical conductivity, as well as providing good support for cell survival and growth during and after 3D bioprinting, which suggests their high application potential for 3D bioprinting in neural tissue engineering.

4D printing, with which 3D printed objects change their shapes over time during application, was introduced in 2013 by Tibbits of the Self-Assembly Lab at the Massachusetts Institute of Technology (MIT)[48,49] and is now increasingly applied in TE.[50-54] Considering the final devices for peripheral nerve regeneration are tubular scaffolds (the so-called "nerve conduits") which bridge severed nerve ends, 4D bioprinting of shape-morphing and electrically conductive cell-scaffold constructs for PNS applications should be explored. As shown in our previous studies,[55,56] 4D printed scaffolds could fold automatically within minutes in an aqueous environment at 37°C from original flat scaffolds into the tubular shape. Furthermore, new shape-morphing mechanisms are developed and employed for 4D printed scaffolds,[57] which may be extended to 4D bioprinted cell-laden constructs. It will be highly interesting and can also be challenging to apply 4D bioprinting in neural tissue engineering.

4. Conclusions

In this work, conducive hydrogels based on natural biopolymers were developed by utilizing gelatin, GelMA, and GO. With the addition of GO, GG hydrogels exhibited improved performance in terms of printability and mechanical properties. Furthermore, the inclusion of even a small amount of GO could endow non-conductive GG hydrogels with good electroactivity. With adequate shear viscosity, GO/GG hydrogels could be 3D printed into 3D tissue engineering scaffolds with delicate internal structures and good shape fidelity. rBMSCs

could be incorporated in GO/GG hydrogels to form bioinks, and the new bioinks could be 3D bioprinted into cell-laden constructs with high cell viability. The added GO improved the viability and growth of rBMSCs in GO/GG composite hydrogels during post-bioprinting incubation. Overall, the GO-incorporated gelatin/GelMA hydrogels with excellent biocompatibility and electroactivity show their high potential for 3D bioprinting in neural tissue engineering.

Author contribution statement

Jiahui Lai: Methodology, Investigation, Result analysis, Writing - original draft, Revision; Xiaodie Chen: Methodology, Investigation; Helen H. Lu: Writing, Editing; Min Wang: Methodology, Research supervision, Writing, Editing, Reviewing, Revision.

Conflict of Interest Statement

There are no conflicts of interest to declare.

Acknowledgements

This work was financially supported by Hong Kong Research Grants Council (RGC) through research grants 17200519, 17202921, 17201622 and N_HKU749/22. Assistance provided by members in M. Wang's group and by technical staff in the Department of Mechanical Engineering, Faculty of Dentistry and Electron Microscopy Unit of The University of Hong Kong (HKU) is acknowledged.

References

1. Mironov V, Reis N, Derby B. Review: Bioprinting: A Beginning. Tissue Eng 2006;12(4):631-634; doi: 10.1089/ten.2006.12.631.

2. Murphy VS, Atala A. 3D bioprinting of tissues and organs. Nat Biotechnol 2014;32(8):773; doi: 10.1038/nbt.2958.

3. Murphy SV, De Coppi P, Atala A. Opportunities and challenges of translational 3D bioprinting. Nat Biomed Eng 2019;4(4):370-380; doi: 10.1038/s41551-019-0471-7.

4. Narayan R, Yoo J, Atala A. 3D bioprinting: Physical and chemical processes. Appl Phys Rev 2021;8(3):030401; doi: 10.1063/5.0060283.

5. Mazzocchi A, Soker S, Skardal A. 3D bioprinting for high-throughput screening: Drug screening, disease modeling, and precision medicine applications. Appl Phys Rev 2019;6(1):011302; doi: 10.1063/1.5056188.

6. Lai J, Wang C, Wang M. 3D printing in biomedical engineering: processes, materials, and applications. Appl Phys Rev 2021;8(2):021322; doi: 10.1063/5.0024177.

7. Mota C, Camarero-Espinosa S, Baker MB, et al. Bioprinting: From Tissue and Organ Development to in Vitro Models. Chem Rev 2020;120(19):10547-10607; doi: 10.1021/acs.chemrev.9b00789.

8. Li H, Li N, Zhang H, et al. Three-Dimensional Bioprinting of Perfusable Hierarchical Microchannels with Alginate and Silk Fibroin Double Cross-linked Network. 3D Print Addit Manuf 2020;7(2):78-84; doi: 10.1089/3dp.2019.0115.

9. Zhang L, Zhang H, Wang H, et al. Fabrication of Multi-Channel Nerve Guidance Conduits Containing Schwann Cells Based on Multi-Material 3D Bioprinting. 3D Print Addit Manuf 2022;10(5):1046-1054; doi: 10.1089/3dp.2021.0203.

10. Duan B, Wang M, Lu WW. Three-dimensional Nanocomposite Scaffolds for Bone Tissue Engineering: From Design to Application. Nano LIFE 2012;02(01):1250005; doi: 10.1142/S1793984411000396.

11. Song JQ, Ye XL, Chen WC, et al. 3D Printing of Skeleton Muscle Tissue Engineering Scaffolds. Nano LIFE 2021;11(04):2141007; doi: 10.1142/S1793984421410075.

12. Duan B, Hockaday LA, Kang KH, et al. 3D Bioprinting of heterogeneous aortic valve conduits with alginate/gelatin hydrogels. J Biomed Mater Res A 2013;101(5):1255-1264; doi: 10.1002/jbm.a.34420.

13. Fang Y, Guo Y, Wu B, et al. Expanding Embedded 3D Bioprinting Capability for Engineering Complex Organs with Freeform Vascular Networks. Adv Mater 2023;35(22):2205082; doi: 10.1002/adma.202205082.

14. Hull SM, Lou J, Lindsay CD, et al. 3D bioprinting of dynamic hydrogel bioinks enabled by small molecule modulators. Sci Adv 2023;9(13):eade7880; doi: 10.1126/sciadv.ade788.

15. Yue K, Trujillo-de Santiago G, Alvarez MM, et al. Synthesis, properties, and biomedical applications of gelatin methacryloyl (GelMA) hydrogels. Biomaterials 2015;73:254-271; doi: 10.1016/j.biomaterials.2015.08.045.

16. Chen S, Wang Y, Lai J, et al. Structure and Properties of Gelatin Methacryloyl (GelMA) Synthesized in Different Reaction Systems. Biomacromolecules 2023;24(6):2928-2941; doi: 10.1021/acs.biomac.3c00302.

17. He J, Sun Y, Gao Q, et al. Gelatin Methacryloyl Hydrogel, from Standardization, Performance, to Biomedical Application. Adv Healthc Mater 2023;12(23):2300395; doi: 10.1002/adhm.202300395.

18. Joung D, Lavoie NS, Guo SZ, et al. 3D Printed Neural Regeneration Devices. Adv Funct Mater 2020;30(1):1906237; doi: 10.1002/adfm.201906237.

19. Lozano R, Stevens L, Thompson B, et al. 3D printing of layered brain-like structures using peptide modified gellan gum substrates. Biomaterials 2015;67(C):264-273; doi: 10.1016/j.biomaterials.2015.07.022.

20. Budday S, Nay R, de Rooij R, et al. Mechanical properties of gray and white matter brain tissue by indentation. J Mech Behav Biomed Mater 2015;46:318-330; doi: 10.1016/j.jmbbm.2015.02.024.

21. Shao L, Gao Q, Xie C, et al. Directly coaxial 3D bioprinting of large-scale vascularized tissue constructs. Biofabrication 2020;12(3):035014; doi: 10.1088/1758-5090/ab7e76.

22. Shao L, Gao Q, Xie C, et al. Synchronous 3D Bioprinting of Large-Scale Cell-Laden Constructs with Nutrient Networks. Adv Healthc Mater 2020;9(15):1901142; doi: 10.1002/adhm.201901142.

23. Xavier Mendes A, Moraes Silva S, O'Connell CD, et al. Enhanced Electroactivity, Mechanical Properties, and Printability through the Addition of Graphene Oxide to Photo-Cross-linkable Gelatin Methacryloyl Hydrogel. ACS Biomater Sci Eng 2021;7(6):2279-2295; doi: 10.1021/acsbiomaterials.0c01734.

24. Li L, Qin S, Peng J, et al. Engineering gelatin-based alginate/carbon nanotubes blend bioink for direct 3D printing of vessel constructs. Int J Biol Macromol 2020;145:262-271; doi: 10.1016/j.ijbiomac.2019.12.174.

25. Goklany S. Conductive Nanomaterials used in Bioinks for 3D Bioprinting. Nano LIFE 2021;11(02):2130005; doi: 10.1142/S1793984421300053.

26. Zhong J, Zhou GX, He PG, et al. 3D printing strong and conductive geo-polymer nanocomposite structures modified by graphene oxide. Carbon 2017;117:421-426; doi: 10.1016/j.carbon.2017.02.102.

27. Zhou X, Nowicki M, Cui H, et al. 3D bioprinted graphene oxide-incorporated matrix for promoting chondrogenic differentiation of human bone marrow mesenchymal stem cells. Carbon 2017;116:615-624; doi: 10.1016/j.carbon.2017.02.049.

28. Li H, Wu X, Cheng K, et al. Preparation of graphene oxide with large lateral size and graphene/polyimide hybrid film via in situ "molecular welding" strategy. Mater Lett 2019;237:168-171; doi: 10.1016/j.matlet.2018.11.096.

29. Kang MS, Kang JI, Le Thi P, et al. Three-Dimensional Printable Gelatin Hydrogels Incorporating Graphene Oxide to Enable Spontaneous Myogenic Differentiation. ACS Macro Lett 2021;10(4):426-432; doi: 10.1021/acsmacrolett.0c00845.

30. Li Z, Xiang S, Lin Z, et al. Graphene oxide-functionalized nanocomposites promote osteogenesis of human mesenchymal stem cells via enhancement of BMP-SMAD1/5 signaling pathway. Biomaterials 2021;277:121082; doi: 10.1016/j.biomaterials.2021.121082.

31. Zhang Y, Wang C, Fu L, et al. Fabrication and Application of Novel Porous Scaffold in Situ-Loaded Graphene Oxide and Osteogenic Peptide by Cryogenic 3D Printing for Repairing Critical-Sized Bone Defect. Molecules 2019;24(9):1669; doi: 10.3390/molecules24091669.

32. Zhang J, Eyisoylu H, Qin XH, et al. 3D bioprinting of graphene oxide-incorporated cell-laden bone mimicking scaffolds for promoting scaffold fidelity, osteogenic differentiation and mineralization. Acta Biomater. 2021;121:637-652; doi: 10.1016/j.actbio.2020.12.026.

33. Li H, Liu S, Li L. Rheological study on 3D printability of alginate hydrogel and effect of graphene oxide. Int J Bioprinting 2016;2(2):54-66; doi: 10.18063/IJB.2016.02.007.

34. Sharma A, Gupta S, Sampathkumar TS, et al. Modified graphene oxide nanoplates reinforced 3D printed multifunctional scaffold for bone tissue engineering. Biomater Adv 2022;134:112587; doi: 10.1016/j.msec.2021.112587.

35. Van Den Bulcke AI, Bogdanov B, De Rooze N, et al. Structural and Rheological Properties of Methacrylamide Modified Gelatin Hydrogels. Biomacromolecules 2000;1(1):31-38; doi: 10.1021/bm990017d.

36. Lai J, Wang C, Liu J, et al. Low temperature hybrid 3D printing of hierarchically porous bone tissue engineering scaffolds with in situ delivery of osteogenic peptide and mesenchymal stem cells. Biofabrication 2022;14(4):045006; doi: 10.1088/1758-5090/ac84b0.

37. Ouyang L, Armstrong JPK, Lin Y, et al. Expanding and optimizing 3D bioprinting capabilities using complementary network bioinks. Sci Adv 2020;6(38):eabc5529; doi: 10.1126/sciadv.abc552.

38. Shuai C, Zeng Z, Yang Y, et al. Graphene oxide assists polyvinylidene fluoride scaffold to reconstruct electrical microenvironment of bone tissue. Mater Des 2020;190:108564; doi: 10.1016/j.matdes.2020.108564.

39. Gong C, Kong Z, Wang X. The Effect of Agarose on 3D Bioprinting. Polymers 2021;13(22):4028; doi: 10.3390/polym13224028.

40. Lim KS, Galarraga JH, Cui X, et al. Fundamentals and Applications of Photo-Cross-Linking in Bioprinting. Chem Rev 2020;120(19),10662-10694; doi: 10.1021/acs.chemrev.9b00812.

41. Shin SR, Aghaei-Ghareh-Bolagh B, Dang TT, et al. Cell-laden Microengineered and Mechanically Tunable Hybrid Hydrogels of Gelatin and Graphene Oxide. Adv Mater 2013;25(44):6385-6391; doi: 10.1002/adma.201301082.

42. Chang R, Nam J, Sun W. Effects of Dispensing Pressure and Nozzle Diameter on Cell Survival from Solid Freeform Fabrication–Based Direct Cell Writing. Tissue Eng Part A 2008;14(1):41-48; doi: 10.1089/ten.a.2007.0004.

43. Fedorovich NE, Oudshoorn MH, van Geemen D, et al. The effect of photopolymerization on stem cells embedded in hydrogels. Biomaterials 2009;30(3):344-353; doi: 10.1016/j.biomaterials.2008.09.037.

44. Fedorovich NE, De Wijn JR, Verbout AJ, et al. Three-dimensional fiber deposition of cell-laden, viable, patterned constructs for bone tissue printing. Tissue Eng Part A 2008;14(1):127-133; doi: 10.1089/ten.a.2007.0158.

45. Colosi C, Shin SR, Manoharan V, et al. Microfluidic bioprinting of heterogeneous 3D tissue constructs using low-viscosity bioink. Adv Mater 2016;28(4):677-684; doi: 10.1002/adma.201503310.

46. Billiet T, Gevaert E, De Schryver T, et al. The 3D printing of gelatin methacrylamide cell-laden tissue-engineered constructs with high cell viability. Biomaterials 2014;35(1):49-62; doi: 10.1016/j.biomaterials.2013.09.078.

47. Mironi-Harpaz I, Wang DY, Venkatraman S, et al. Photopolymerization of cell-encapsulating hydrogels: Crosslinking efficiency versus cytotoxicity. Acta Biomater 2012;8(5):1838-1848; doi: 10.1016/j.actbio.2011.12.034.

48. Tibbits S. The emergence of "4D printing". TED Conference 2013, available from: https://www.ted.com/talks/skylar_tibbits_the_emergence_of_4d_printing (Last accessed: 11/2/2023).

49. Tibbits S. 4D printing: multi-material shape change. Archit Des 2014;84(1):116-121; doi: 10.1002/ad.1710.

50. Wang Y, Cui H, Wang Y, et al. 4D Printed Cardiac Construct with Aligned Myofibers and Adjustable Curvature for Myocardial Regeneration. ACS Appl Mater Interfaces 2021;13(11):12746-12758; doi: 10.1021/acsami.0c17610.

51. Lai J, Wang M. Developments of additive manufacturing and 5D printing in tissue engineering. J Mater Res. 2023; doi: 10.1557/s43578-023-01193-5.

52. Chen X, Han S, Wu W, et al. Harnessing 4D Printing Bioscaffolds for Advanced Orthopedics. Small 2022;18(36):2106824; doi: 10.1002/smll.202106824.

53. Zhang X, Yang Y, Yang Z, et al. Four-Dimensional Printing and Shape Memory Materials in Bone Tissue Engineering. Int J Mol Sci 2023;24(1), 814; doi: 10.3390/ijms24010814.

54. Zhao YD, Lai JH, Wang M. 4D Printing of Self-Folding Hydrogel Tubes for Potential Tissue Engineering Applications. Nano LIFE 2021;11(04):2141001; doi: 10.1142/S1793984421410014.

55. Lai J, Li J, Wang M. 3D Printed porous tissue engineering scaffolds with the self-folding ability and controlled release of growth factor. MRS Commun. 2020;10(4):579-586; doi: 10.1557/mrc.2020.65.

56. Wang C, Yue H, Liu J, et al. Advanced reconfigurable scaffolds fabricated by 4D printing for treating critical-size bone defects of irregular shapes. Biofabrication 2020;12(4):045025; doi: 10.1088/1758-5090/abab5b.

57. Lai J, Ye X, Liu J, et al. 4D printing of highly printable and shape morphing hydrogels composed of alginate and methylcellulose. Mater Des 2021;205:109699; doi: 10.1016/j.matdes.2021.109699.